TRANSACTIONS OF THE INSTITUTE OF FLUID-FLOW MACHINERY

No. 133, 2016, 117–129

Jakub Łagodziński*, Piotr Zieliński

A combined numerical-experimental model of air foil bearing compliant structure

Institute of Turbomachinery, Lodz University of Technology,
219/223 Wólczańska, 90-924 Łódź, Poland

Abstract

The paper concerns the development process of numerical-experimental model of air foil bearing compliant structure. Theoretically, static and dynamic characteristics of the foil bearing are the result of elastic combined properties of the two serially connected elements. One of them is a thin gas film of very small thickness and relatively high static and dynamic stiffness. The second elastic element is a pretensioned bump foil spring. This paper focuses on the properties of compliant foil structure and leaves aside the gas film behavior. At the beginning of the model development, the global stiffness and damping properties of compliant structure were obtained from the test stand measurements. In the next step, some assumptions concerning the model were made. The main one was the replacememy of the single bumps of the corrugated foil by the set of elastic-damping numerical elements. At last, the fine-tuning of the model was carried out. The tuning involved changing of subelements local damping and stiffness properties, which in effect influenced the global properties of foil bearing. The tuning criterion for the model was defined as follows: the bearing global stiffness and damping properties of the model should not differ from the experimentally obtained values more than 10%.

Keywords: Airfoil bearing; Numerical model; Gas bearing coefficients

1 Introduction

The gas foil bearings are a type of aerodynamic bearings that utilize air as their lubricating medium. The name 'foil' comes from their design (Fig. 1), because the shaft is supported in a thin metal foil structure that is mounted in the bearing

*Corresponding Author. Email adress: jakub.lagodzinski@p.lodz.pl

sleeve. At high rotational speed, a gas film occurs between the shaft and the foil structure. The first foil bearing was designed and built in 1953 but that concept wasn't able to compete with commonly used bearings. The main drawback was the lack of a proper coating layer. The coating layer in the foil bearing ensures low friction coefficient and ability to withstand contact conditions during startup and shutdown. The foil bearings found their first successful applications in aerospace industry. In 1969 an air cycle machine from the McDonnell Douglas DC-10 jet airlinerwas supported in foil bearings and fulfilled engineers expectations. Since that time foil bearings evolve through many concepts and found many applications but the base structure did not change much.

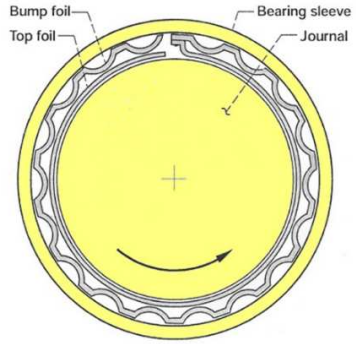

Figure 1: Foil bearing structure [1].

Foil bearing operation is similar to oil hydrodynamic bearings but the working fluid is not oil but air which results in many advantages as well as disadvantages. The top foil is responsible for proper forming of the gas film. The bump foil clenches the top foil around the shaft. This pre-clamp provides higher bearing load capacity, but on the other hand increases frictional torque during the start-up. Using air as the lubricating medium simplifies the foil bearing construction, and moreover, no other device like supply pump or compressor is needed. Low viscosity of air results in minimal bearing losses, however lower viscosity means also lower bearing load capacity. One of the most important disadvantages is friction between shaft and top foil during run-up and run-down of machine, when rotation speed is low. Difference between oil and foil bearing is shown in Fig. 2.

Correctly operating foil bearings are design solutions that have wide possibilities of applications, unavailable for rolling or oil bearings [1]. Nowadays in many scientific centers in the world, the main research on foil bearings is devoted to elimination of their basic disadvantages such as high start-up moment and wear

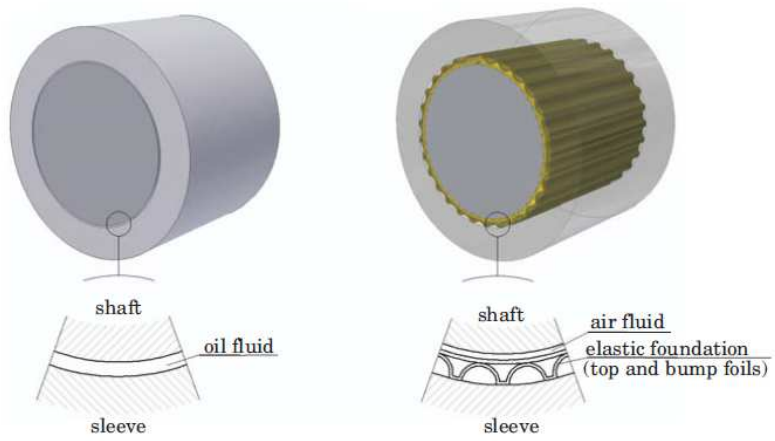

Figure 2: Difference between oil and foil bearings [6].

of component surfaces. The next important goal is to predict and design properly the behavior of a complex support system consisting of the gas film and the compliant – damping foil structure. This can be achieved by building a trustworthy foil bearing dynamic model that accurately imitates the real bearing properties. The complexity of the theoretical model of such a bearing is deepened by the issue of the relative motion of both foils and the friction of the bump and cylindrical foils that takes place [2,3].

2 Dynamic properties of the compliant structure of the bump foil bearing

Theoretically, static and dynamic characteristics of the foil bearing are the result of elastic combined properties of the two elements serially connected (see Fig. 3). One of them is a thin gas film of very small thickness and relatively high static and dynamic stiffness, K_G. The second elastic element is a pretensioned bump foil spring with stiffness, K_F, and damping, C_F.

It should be noticed that depending on the bump foil pre-tension, a stiff gas film appears for speeds from few thousand to over a several dozen kilos revolutions per minute. Above this speed limit, a continuous gas film occurs, and the foil bearing operates properly when the rotating journal loses contact with the top foil.

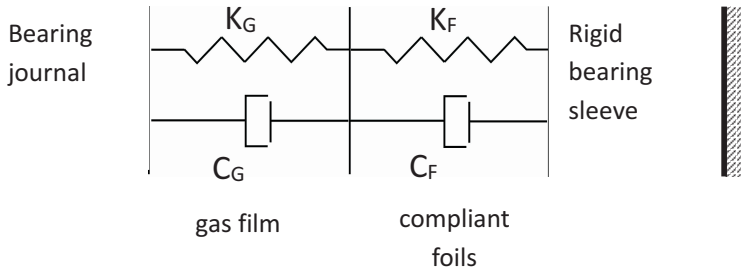

Figure 3: Simplified physical model of the bump foil bearing [7].

The accepted physical model of the start-up of aerodynamic foil bearings allows one to formulate the following statements:

- for the journal rotational speed below n_{lim}, where n_{lim} denotes the rotational speed at which the continuous gas film appears, it can be assumed that the dynamic properties of the bearing depend on the stiffness of bump foil springs, because $K_G \ll KF$;
- at the journal rotational speed above n_{lim}, theoretically, the dynamic properties of the support system depend on the combined stiffness of the two elements serially connected.

The complexity of the analysis of the foil bearing theoretical model is caused by friction between the bump foil and the sleeve and between both foils. The friction comes from a relative motion of the foils and a relative motion of the bump foil and the sleeve. This physical phenomenon results in highly nonlinear dynamic properties of the foil bearing support system [4,5].

Some experimental attempts were made to identify these properties and a foil bearing test rig was built for this purpose (Fig. 4). The test rig consisted of a fixed journal, frictionlessly supported sleeve and a modal shaker. The sleeve of 1.6 kg weight was excited with a sinusoidal waveform force by the shaker to simulate real synchronous excitation caused by rotor unbalance. During the experiment, the excitation force and the sleeve displacement were measured. The measured object was a foil structure of third+ generation bearing. The dimensions of the bearing were $\phi 34 \times 40$.

A typical response of the shaking system is a hysteresis loop, presented in Fig. 5. From this image, one can obtain the bump spring overall stiffness, k, and an area of the hysteresis loop, W, which represents the energy dissipated in a single motion cycle. The energy dissipation is related to the friction between the

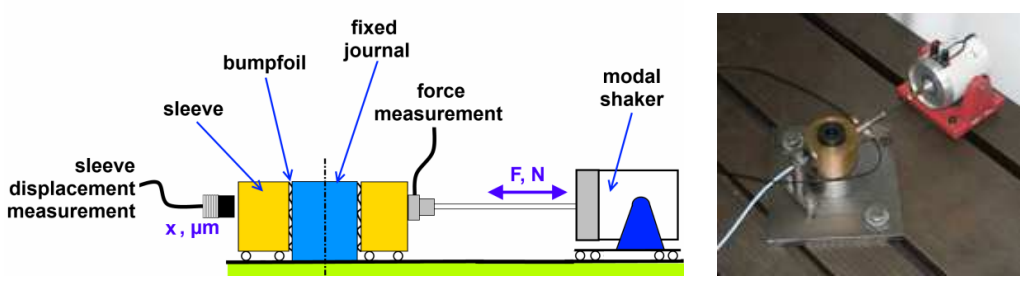

Figure 4: Functional diagram and a photo of the test rig built for the experimental identification of dynamic properties of the third+ generation foil bearing support structure [7].

bearing foils and can be estimated from:

$$W = \oint F dx \ = \pi \omega C_{eq} X^2 \,, \tag{1}$$

where: W – area of the hysteresis loop, F – force amplitude, x – displacement, X – vibration amplitude, ω – circular frequency. Transforming Eq.(1) one can obtain the equivalent damping coefficient.

$$C_{eq} = \frac{W}{\pi \, \omega \, X^2} \,. \tag{2}$$

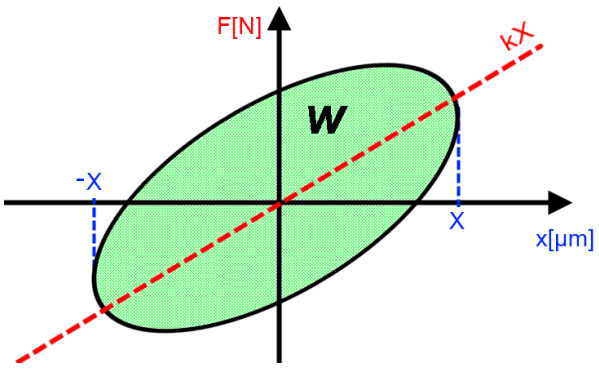

Figure 5: Image response as a hysteresis loop associated with friction and elasticity of the compliant foil bearing assembly [7].

During measurements foil structure was subjected to sinusoidal force at three values of force per one excitation frequency. Six different frequencies from range 100 to 600 Hz were applied. The applied excitation force and the bearing amplitude

were measured. An important parameter during measurements was sampling frequency. To avoid aliasing, the sampling frequency was at least forty times higher than excitation frequency. The range of applied excitation forces is shown in Tab. 1.

Table 1: Measurement program

Sampling rate, Hz	Excitation frequency, Hz	Amplitude of excitation force, N		
5000	100	5	7	10
10000	200	5	7	10
12500	300	5	7	10
25000	400	5	7	10
25000	500	5	7	10
25000	600	5	7	10

3 Numerical model

The model of foil structure was written in commercial software ANSYS Parametric Design Language 16.1 [11] to imitate the real foil bearing. Similarly to the test rig, the shaft is fixed to the support, and the bearing sleeve in the model is excited by sinusoidal force applied to node 49 (see Fig 6). The mass of the sleeve equals to 1.6 kg and is focused also in node 49. The sleeve was considered to be rigid in comparison to the foil structure. Every single bump of the bumpfoil in bearing was simulated by two COMBIN14 elements which have their own internal damping and stiffness coefficients. By changing these coefficients the model behaviour can be adjusted to the measurement results for each configuration of frequency depend on the excitation force. The main goal was to adjust model to measurement results with 10% aberration margin, although it was impossible in some cases. Schematics diagram and realization in ANSYS are shown in Fig. 7. The whole model of foil bearing is shown in Fig. 6.

4 The comparison results

Figure 8 presents the amplitude response of the bearing model to sudden application of sinusoidal force at substep 1 (for time $t = 0$ s). As can be observed, the

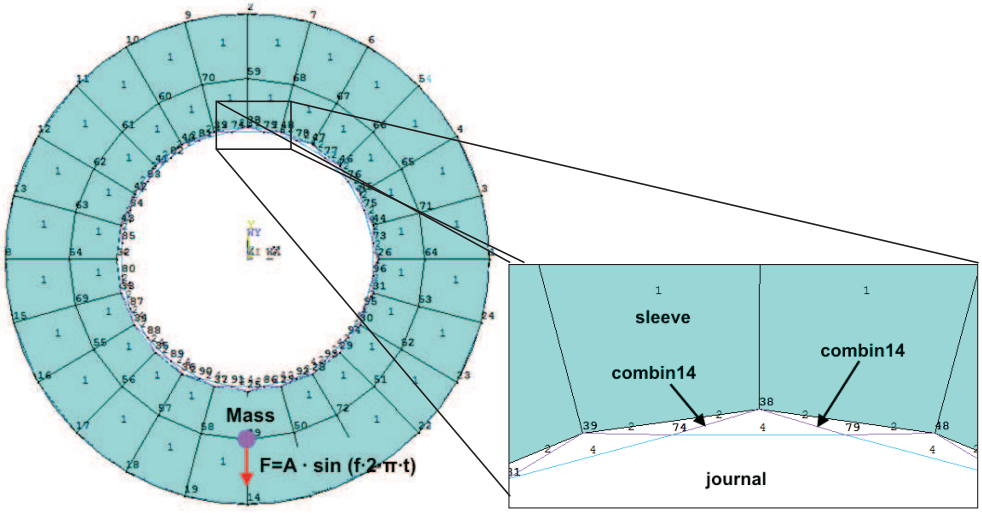

Figure 6: Numerical model of the full foil bearing. On the right: zoom of the modeled structure of the bump foil.

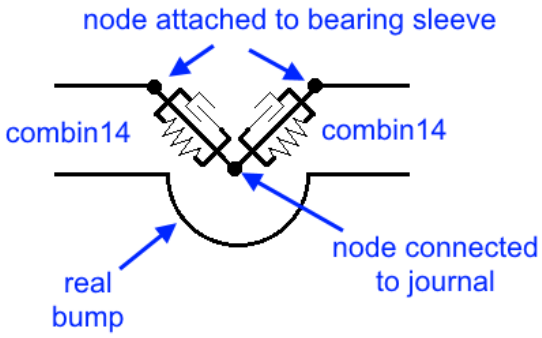

Figure 7: A simplified model of single bump represented by two COMBIN14 elements.

model achieves stable amplitude after approx. 1000 substeps. For more reliable results, the hysteresis loop from above 1500th substep was taken for a comparison with the experimental results. A representative response is presented in Fig. 9. This is an exemplary result for frequency $f_{ex} = 100$ Hz and force $F_{ex} = 5$ N. The diagram shows two histeresis loops: one obtained from the experiment (the solid line) and the other obtained from the model adjustment (the dotted line).

The model and measurement comparative analyses were conducted for each

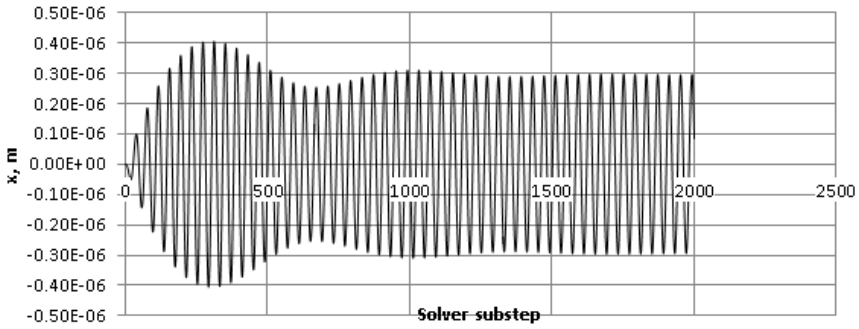

Figure 8: Amplitude of model sleeve vs. number of substep. Exemplary results for frequency $f_{ex} = 100$ Hz and force $F_{ex} = 5$ N.

frequency. The comparison covered few important bearing properties, i.e., the global damping coefficient, the global stiffness, the dissipated energy and minimal, maximal and mean amplitude. Results of a comparative analysis for 100 Hz are shown in Tab. 2.

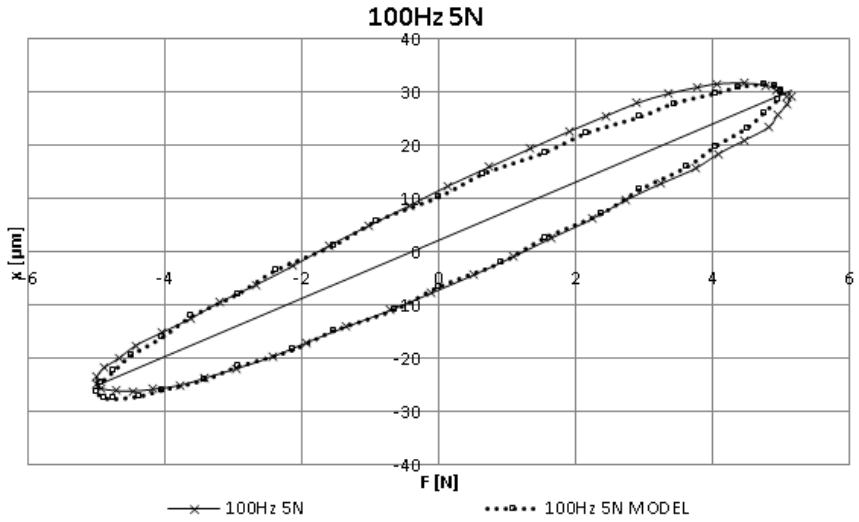

Figure 9: Hysteresis loops obtained from both numerical model and from measurement.

Table 2: Result of comparative analysis for frequency of 100 Hz.

Force [N]	Item	Dissipated energy [μJ]	Maximal amplitude [μm]	Minimal amplitude [μm]	Mean amplitude [μm]	Damping coefficient [N s/m]	Overall stiffness [N/m]
5	Measurement	146.705	31.720	-26.070	28.895	89.016	182809
	Model	138.069	31.453	-27.437	29.445	80.675	170268
	Deviation	-5.89%	-0.84%	5.24%	1.90%	-9.37%	-6.86%
7	Measurement	213.933	57.380	-46.180	51.780	40.423	139119
	Model	215.731	54.072	-46.065	50.068	43.597	143798
	Deviation	0.84%	-5.77%	-0.25%	-3.31%	7.85%	3.36%
10	Measurement	1225.685	101.150	-69.330	85.240	85.460	138443
	Model	931.204	87.878	-73.922	80.900	43.597	143798
	Deviation	-24.03%	-13.12%	6.62%	-5.09%	-15.66%	-4.24%

5 Results discussion

The comparative analysis covered the whole spectrum of measurements described in Tab. 1. After obtaining the experimental object properties, the tuning of the model was performed. This allowed obtaining the model that accurately behaves like a real object. The values of global stiffness and damping coefficients for both model and real object are presented in Figs. 10 and 11.

As one can see in above figures, damping is dropping significantly for frequency 500 Hz. However, for 600 Hz it is almost three times higher than the average from range 100 to 400 Hz. Such behaviour of the foil structure is favourable, because foil bearings usually work with high rotation speed machines and we can expect that this coefficient has a rising tendency for frequencies higher than 600 Hz. Stiffness coefficient in the range from 100 to 500 Hz has almost linear rising tendency and differences between excitation forces are minimal. In that range, the stiffness coefficient depends only on frequency. For 600 Hz, it reaches the highest value for each excitation force and for that frequency we can see that the coefficient depends not only on the frequency but also on the excitation force. The unique nonlinear behaviour of the foil structure is quite interesting and in further studies should be examined thoroughly.

The numerical model in most cases was quite easy to tune its behaviour to experimental performance of the real bearing. The results are shown in Figs. 12 and 13. One of the most important conclusions concerns the applied values of

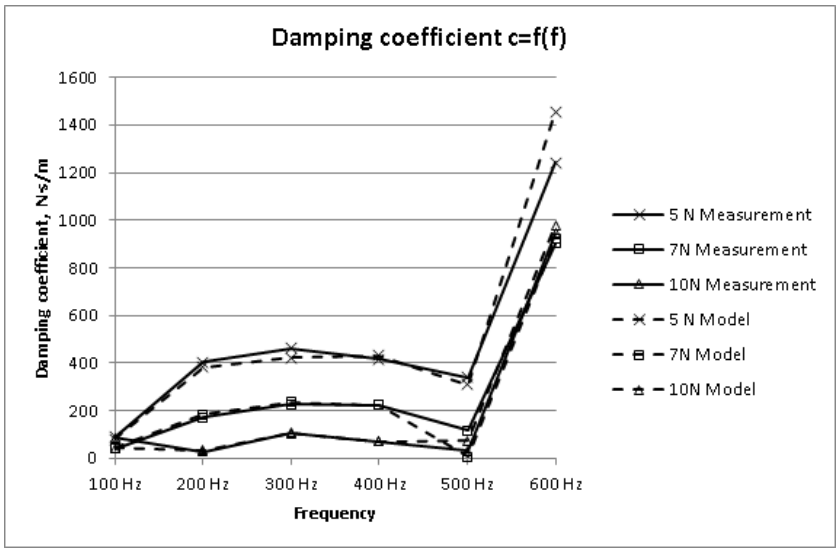

Figure 10: Global bearing damping coefficient versus excitation frequency.

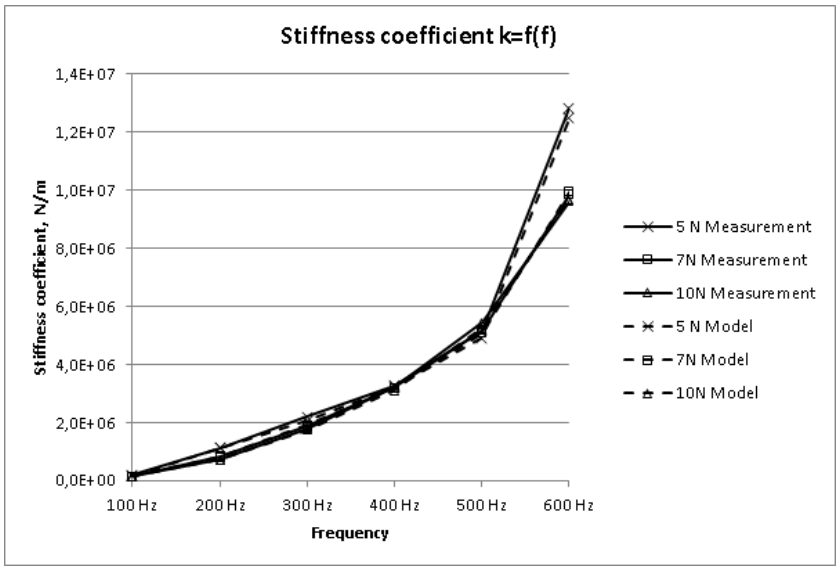

Figure 11: Global bearing stiffness coefficient in function of excitation frequency.

COMBIN14 element coefficients responsible for stiffness and damping. As we can see in above figures, that applied damping coefficient of COMBIN14 element has

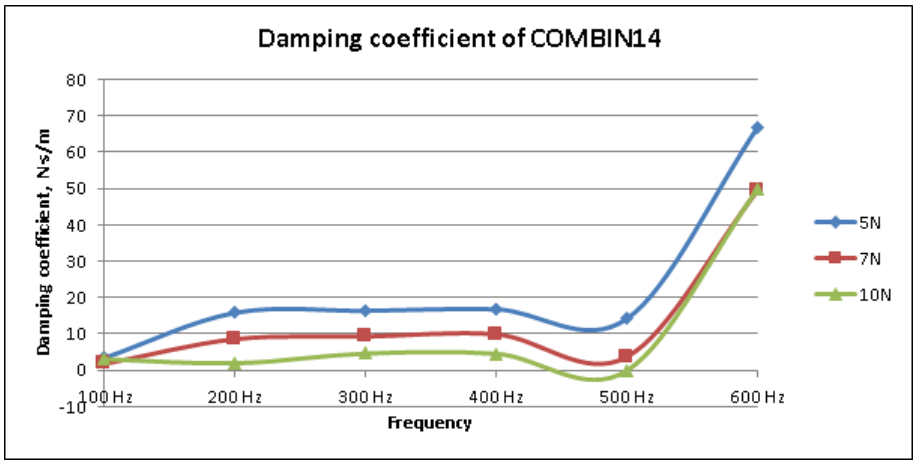

Figure 12: Damping coefficient of COMBIN14 element in function of the excitation frequency.

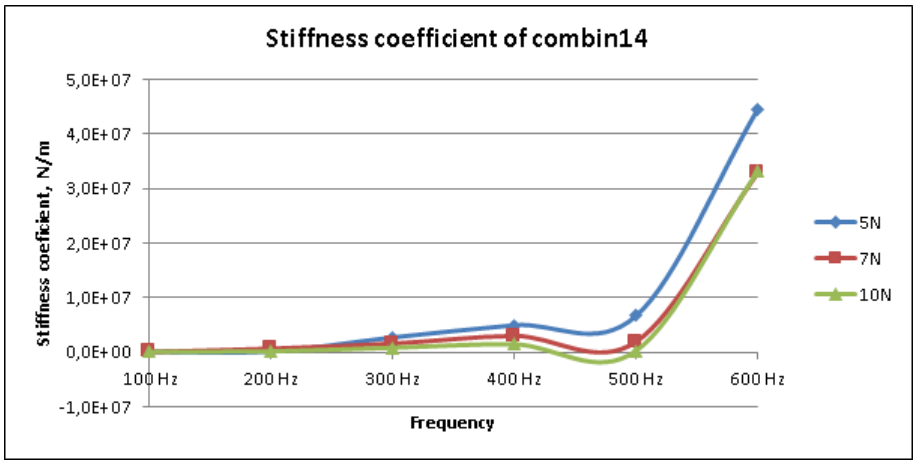

Figure 13: Stiffness coefficient of COMBIN14 element in function of excitation frequency.

similar curve as the global damping coefficient presented in Fig. 10. In the other hand, the applied stiffness coefficient values of single COMBIN14 do not imitate the values of global stiffness of the bearing, but the obtained stiffness curve looks very similar to the damping coefficient curve which is really interesting.

We also check if there is any simple relation between COMBIN14 and real bearing global coefficients. This was done by dividing one by another, allowing describing them by using easy equation. The quotient of damping coefficients was called A_1, and the quotient of stiffness coefficients was called A_2. Results are pre-

sented in Figs. 14 and 15. As we can see the simple relation does not exist, which indicates that model is too simple to be useful for engineering purposes. Never the less, we see that for 600 Hz factors A_1 and A_2 depend only on frequency, what leads to the conclusion that for higher frequencies, the COMBIN14 coefficients could be more useful to describe a reliable numerical model of airfoil bearing.

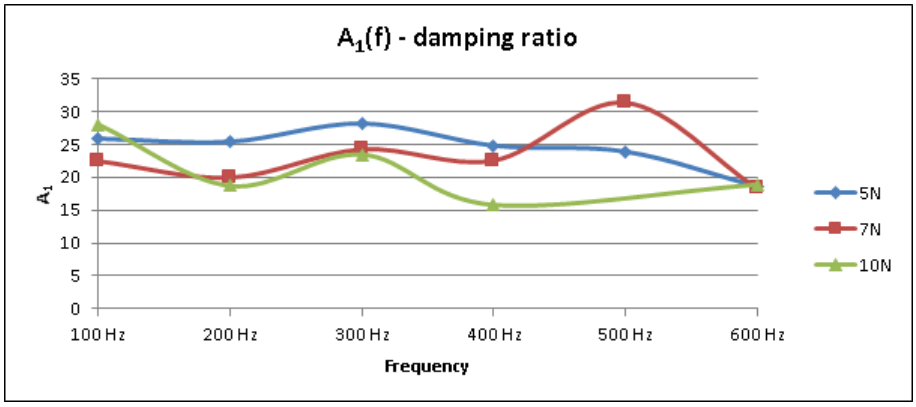

Figure 14: Result quotient of measured global bearing and COMBIN14 element damping coefficients.

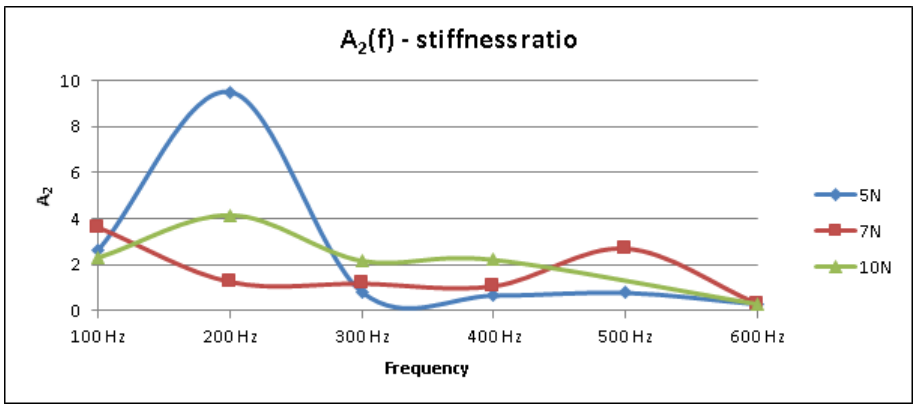

Figure 15: Result quotient of global bearing and COMBIN14 element stiffness coefficients.

6 Conclusion

Measurements of foil structure parameters indicate that better operational ones at high speed rotation are not the only result of gas aerodynamic reaction. It can be observed that with the rising frequency, stiffness and damping coefficient of foil structure increases. It will be a good idea to check that structure in a wider range of frequencies in the future, because the most interesting results show at the end of the measure range. Due to the limitation of the modal shaker, it is not possible at present.

Received in July 2016

References

[1] Andres L., Rubio D., Kim T.: *Rotordynamic performance of a rotor supported on bump type foil bearings: experiments and predictions*. ASME Turbo Expo, Barcelona 2006, GT2006-91238.

[2] Kicinski J. Żywica G.: *The numerical bearings*. Adv. Vib. Eng. **11**(2012), 2, 113–119.

[3] Kozanecki Z., Kozanecka D. *Theoretical and experimental investigations of oil-free support systems to improve the reliability of industrial turbomachinery*. In: Proc. 8th IFTOMM Int. Conf. on Rotor Dynamics. Sept. 12-15, 2010/KIST, Seoul, 686–692.

[4] Kozanecka D., Kozanecki. Z., Łagodziński J., Tkacz E.: *Experimental research of oil-free support systems to predict the high-speed rotor bearing dynamics*. Int. J. Dynamics and Control, Springer Verlag Berlin Heidelberg (2014), DOI 10.1007/s40435-014-0074-9.

[5] Łagodziński J., Kozanecki Z., Tkacz E., Miazga K.: *Theoretical and experimental investigations of oil-free bearings and their application in diagnostics of high-speed turbomachinery*. Key Eng. Mat. **588**(2014), 302–309 online available since 2013/oct/11 at www.scientific.net (2014) Trans Tech Publications, Switzerland DOI:10.4028/www.scientific.net/kem.588.302.

[6] Żywica G., *The dynamic performance analysis of the foil bearing structure*. Acta Mechanica et Automatica **7**(2013, 1 , 58–62, DOI 10.2478/ama-2013-0011.

[7] Kozanecki Z., Łagodziński J., Tkacz E., Miazga K.:*Oil-free bearings for hermetic high-speed turbomachinery*. J. Vib. Eng. Technol. **2**(2014), 4, (accessed Jan. 09, 2015).

[8] Dessornes O., Landais S., Valle R., Fourmaux A., Burguburu S., Kozanecki Z. *et al.*: *Advances in the development of a microturbine engine*. J. Eng. Gas Turbines and Power **136**(2014), 7.

[9] Kozanecki, Z. Kiciński J., Żywica G.: *Numerical model of the high speed rotors supported on variable geometry bearings*. In: Proc. IUTAM Symp. on Emerging Trends in Rotor Dynamics (March 23–26, 2009 New Delhi, India), Springer Verlag, 2007.

[10] DellaCorte C.: *Oil-free shaft support system rotordynamics: Past, present and future challenges and opportunities*. Mech. Systems Signal Process. **29**(2012), 67-76.

[11] *ANSYS Parametric Design Language Guide*. ANSYS Inc. Release 14.5, October 2012.